An efficient wave based method for 2D dynamic poroelastic problems with corner stress singularities

E. Deckers, D. Vandepitte, W. Desmet
K.U.Leuven, Department of Mechanical Engineering,
Celestijnenlaan 300 B, B-3001, Heverlee, Belgium
e-mail: **Elke.Deckers@mech.kuleuven.be**

Abstract

Recently, a wave based method was developed to efficiently model the harmonic behavior of poroelastic materials. This novel method relaxes the frequency limitations of the finite element method by using exact solutions of the governing equations to approximate the field variables. However, in the case that the stress fields exhibit a singularity, the Wave Based Method suffers from convergence problems. This paper derives criteria to predict the presence of stress singularities in poroelastic problem domains and proposes a suitable set of enrichment functions to extend the conventional set of expansion functions. The beneficial effect of incorporating these functions on the convergence of the Wave Based Method is illustrated by means of a numerical validation study.

1 Introduction

The most commonly applied mathematical model to describe the dynamic behavior of poroelastic materials is the Biot theory [1, 2]. Using a set of two frequency-dependent coupled partial differential equations, this constitutive model predicts the existence of three different fluid-frame coupled wave types: a shear wave and two compressional waves.

Currently, the Finite Element Method (FEM) is the most commonly used prediction technique for the steady-state dynamic analysis of poroelastic materials. Even though several alternative formulations exist [3, 4, 5], these calculations are very time-consuming due to the complex and frequency dependent material properties, the high number of unknowns per node and the dense problem discretizations needed to capture the short wavelengths in the poroelastic response fields at higher frequencies. As a result, the use of the FEM is practically limited to low-frequency applications [6].

The Wave Based Method (WBM) [7] is an alternative deterministic method which is based on the Trefftz principle [8]. Instead of discretizing the problem domain into a large number of small elements, the WBM partitions the problem domain into a small number of large, convex subdomains. In each subdomain, the dynamic response variables are approximated using so-called wave functions which are exact solutions of the governing differential equations. In this way, the wave functions may only violate the boundary and continuity conditions. Enforcing the errors on the boundaries and interfaces to zero through a weighted residual formulation yields a small matrix equation which can be solved for the contribution factor of each wave function. The authors have recently proposed a WBM for the solution of the Biot equations [9, 10]. The dynamic field variables are approximated using a superposition of three types of globally defined wave functions, corresponding to the three aforementioned poroelastic wave types. By embedding a priori knowledge in the numerical scheme a significant increase in modeling efficiency is realized and accurate response predictions in an extended frequency range become feasible.

Due to the linearized underlying constitutive model, the poroelastic stress fields may become infinite at discontinuities along the problem boundary. When using the FEM, these phenomena do not interfere with the overall prediction accuracy due to the local support of the FE shape functions. In the WB approach, a more profound impact on the predicted response fields is observed due to the global nature of the applied approximation functions. A possible solution to cope with these problems which obviously impact the convergence rate is to extend the set of wave functions using some additional enrichment functions, which accurately represent the singular behavior of the dynamic fields near the corner point. Similar to the work by Vanmaele et al. [11, 12] on the treatment of corner stress singularities in plate bending and plate membrane problems, a set of generic criteria for the presence of stress singularities in the poroelastic responses based on the internal angle of each corner and the applied boundary conditions is derived. Using an asymptotic response analysis a suitable set of enrichment functions is proposed. The beneficial effect of incorporating these functions in the field variable approximations on the convergence of the WBM is illustrated by means of a numerical validation study.

This paper is organized as follows. Section 2 discusses the mathematical formulation of a general two-dimensional poroelastic problem and presents the most commonly applied boundary conditions. Section 3 addresses the WB modeling approach and applies it to 2D poroelastic problems. Section 4 deals with the existence of stress singularities in a poroelastic domain and derives enrichment functions to capture the singular behavior at corner points of a poroelastic domain. The use of the WBM for poroelastic materials is demonstrated in section 5 and it is shown that adding the enrichment functions to the set of wave functions is beneficial for the convergence rate of the method. The paper ends with some concluding remarks and topics for future research.

2 Problem definition

A poroelastic material consists of a solid phase ($\bullet^s$) which interacts with the fluid phase ($\bullet^f$) contained within its pores. The Biot theory [1] assumes that the pores are homogenously distributed in the material and uses an equivalent solid and a compressible fluid continuum description on a macroscopic level. This is justified in the case that the typical pore dimensions are very small as compared to the wavelengths of the different types of waves which propagate through the material. The dynamic equations are:

$$N\nabla^2\mathbf{u^s}(\mathbf{r}) + \nabla[(\lambda + \frac{Q^2}{R} + N)e^s(\mathbf{r}) + Qe^f(\mathbf{r})] = -\omega^2(\rho_{11}^*\mathbf{u^s}(\mathbf{r}) + \rho_{12}^*\mathbf{u^f}(\mathbf{r})) \tag{1}$$

$$\nabla[Qe^s(\mathbf{r}) + Re^f(\mathbf{r})] = -\omega^2(\rho_{12}^*\mathbf{u^s}(\mathbf{r}) + \rho_{22}^*\mathbf{u^f}(\mathbf{r})) \tag{2}$$

Appendix A contains a description of the material properties of porous materials and the notations used in this paper. For a complete description and interpretation of the material properties, the equilibrium and the constitutive equations, the reader is referred to literature [2, 3, 7, 10].

Three boundary conditions have to be specified at each point of the boundary in order to have a well-posed problem. The boundary of the subdomain, Γ_{pe}, consists of three non-overlapping parts ($\Gamma_{pe} = \Gamma_{ki} \bigcup \Gamma_{me} \bigcup \Gamma_{mi}$) along which one of the three following sets of boundary residuals are defined:

- kinematic boundary conditions, the displacement components are prescribed:

$$\mathbf{r} \in \Gamma_{ki} : \begin{cases} R_{u_n^s}(\mathbf{r}) = u_n^s(\mathbf{r}) - \bar{u}_n^s(\mathbf{r}) = 0 \\ R_{u_s^s}(\mathbf{r}) = u_s^s(\mathbf{r}) - \bar{u}_s^s(\mathbf{r}) = 0 \\ R_{u_n^f}(\mathbf{r}) = u_n^f(\mathbf{r}) - \bar{u}_n^f(\mathbf{r}) = 0 \end{cases} \tag{3}$$

  with $\bar{u}_n^s(\mathbf{r})$, $\bar{u}_s^s(\mathbf{r})$ and $\bar{u}_n^f(\mathbf{r})$ respectively the prescribed values of the displacement components of the solid phase in the normal and tangential direction to the boundary and the prescribed value of the displacement of the fluid phase in the normal direction to the boundary.

- mechanical boundary conditions, the stress resultants are prescribed:

$$\mathbf{r} \in \Gamma_{me} : \begin{cases} R_{\sigma_n^s}(\mathbf{r}) = \sigma_n^s(\mathbf{r}) - \bar{\sigma}_n^s(\mathbf{r}) = 0 \\ R_{\sigma_s^s}(\mathbf{r}) = \sigma_s^s(\mathbf{r}) - \bar{\sigma}_s^s(\mathbf{r}) = 0 \\ R_{\sigma^f}(\mathbf{r}) = \sigma_n^f(\mathbf{r}) - \bar{\sigma}^f(\mathbf{r}) = 0 \end{cases} \tag{4}$$

  with $\bar{\sigma}_n^s(\mathbf{r})$, $\bar{\sigma}_s^s(\mathbf{r})$ and $\bar{\sigma}^f(\mathbf{r})$ respectively the prescribed values of the normal and tangential stress resultant components of the solid phase in the normal and tangential direction to the boundary and the prescribed hydrostatic stress of the fluid phase.

- mixed boundary conditions:

$$\mathbf{r} \in \Gamma_{mi} : \begin{cases} R_{u_n^s}(\mathbf{r}) = u_n^s(\mathbf{r}) - \bar{u}_n^s(\mathbf{r}) = 0 \\ R_{u_n^f}(\mathbf{r}) = u_n^f(\mathbf{r}) - \bar{u}_n^f(\mathbf{r}) = 0 \\ R_{\sigma_s^s}(\mathbf{r}) = \sigma_s^s(\mathbf{r}) - \bar{\sigma}_s^s(\mathbf{r}) = 0 \end{cases} \tag{5}$$

  For a sliding edge, the prescribed values of $\bar{u}_n^s(\mathbf{r})$, $\bar{u}_n^f(\mathbf{r})$ and $\bar{\sigma}_s^s(\mathbf{r})$ are zero.

3 The Wave Based Method for poroelastic problems

First, this section introduces the methodology of the WBM for a general 2D convex bounded Helmholtz problem. The general problem setting and the basic concept are explained. Afterwards the WBM is applied to the specific case of poroelastic problems.

3.1 General problem setting

Consider a general two-dimensional bounded steady-state dynamic problem Ω. The mathematical formulation of the physics in Ω results in (a coupled system of) N_H second-order Helmholtz equation(s):

$$\nabla^2 u_j(\mathbf{r}) + k_j^2 u_j(\mathbf{r}) = \mathcal{F}_j(\mathbf{r}),\ \mathbf{r} \in \Omega,\ j = 1, ..., N_H \tag{6}$$

In this equation, ∇^2 is the Laplacian operator, k_j is the physical wave number of the j^{th} Helmholtz equation, which is determined by the physical properties of the medium inside the problem domain Ω. $\mathcal{F}_j(\mathbf{r})$ represents non-homogenous forcing terms. The boundary of the total interior problem Γ_b can be divided into non-overlapping parts: $\Gamma_b = \bigcup_i \Gamma_i$, on which different boundary conditions can be imposed. The boundary conditions can be written in the general form:

$$\mathcal{B}_i(u_j(\mathbf{r})) = \overline{\mathcal{B}}_i(\mathbf{r}),\ \mathbf{r} \in \Gamma_i \tag{7}$$

with $\mathcal{B}_i(\bullet)$ a general boundary differential operator and $\overline{\mathcal{B}}_i(\mathbf{r})$ an imposed boundary field. The Helmholtz equation(s) (6) together with the applied boundary conditions (7) along Γ_b defines a unique dynamic field $u_j(\mathbf{r})$ in the problem domain Ω.

3.2 Basic concept of the WBM

The WBM [7] is a deterministic numerical method and belongs to the family of indirect Trefftz [8] approaches. Unlike the FEM, the WBM partitions the problem domain into a limited number of large convex subdomains. Convexity of the subdomains is a sufficient condition for the method to converge towards the exact solution of the problem [7]. Within each subdomain, the dynamic field variables are approximated using an set of wave functions which intrinsically satisfy the governing Helmholtz equation(s). The degrees of freedom (dofs) are the contribution factors of each wave function in this expansion. Enforcing the boundary

and interface conditions along the subdomain boundaries using a Galerkin weighted residual formulation leads to a small, complex and frequency dependent system of equations which can be solved for the contribution factor of each wave function. The general modeling procedure of the WBM consists of the following 4 steps:

1. Partitioning of the considered problem domain into convex subdomains
2. Selection of a suitable set of wave functions for each subdomain
3. Construction of the WB system matrices via a weighted residual formulation of the boundary and interface conditions
4. Solution of the system of equations, yielding the wave function contribution factors and postprocessing of the dynamic variables

3.2.1 Domain partitioning

If the problem domain Ω is non-convex, a partitioning into N_Ω non-overlapping convex subdomains is required, since the convexity of the considered problem domain is a sufficient condition for the theoretical convergence of the WBM [7]. Continuity conditions have to be imposed on the interfaces between adjacent subdomains. For sake of simplicity and to keep the focus on the treatment of stress singularities, we will only consider convex problem domains in this paper. A general description of continuity conditions is given in [7, 13].

3.2.2 Field variable expansions

The steady-state dynamic field(s) $u_j(\mathbf{r})$ in the problem domain Ω are approximated by a solution expansion $\hat{u}_j(\mathbf{r})$ in terms of n_w wave functions Φ_w:

$$u_j(\mathbf{r}) \simeq \hat{u}_j(\mathbf{r}) = \sum_{w=1}^{n_w} u_w \Phi_w(\mathbf{r}) + \hat{u}_{p,j}(\mathbf{r}) = \mathbf{\Phi_w}(\mathbf{r})\ \mathbf{u_w} + \hat{u}_{p,j}(\mathbf{r}). \tag{8}$$

The wave function contribution factors u_w belonging to each of the wave functions are gathered in the vector of degrees of freedom $\mathbf{u_w}$. $\hat{u}_{p,j}(\mathbf{r})$ represents a particular solution resulting from the combined source terms $\mathcal{F}_j(\mathbf{r})$ in the right hand side of the inhomogeneous Helmholtz equation (6).
The row vector $\mathbf{\Phi_w}(\mathbf{r})$ collects the n_w wave functions $\Phi_w(\mathbf{r})$. Each wave function $\Phi_w(\mathbf{r})$ exactly satisfies the homogeneous part of the Helmholtz equation (6). For two-dimensional bounded domains, two sets of wave functions are distinguished, the r- and the s-set:

$$\sum_{w=1}^{n_w} u_w \Phi_w(\mathbf{r}) = \sum_{w_r=1}^{n_{w_r}} u_{w_r} \Phi_{w_r}(\mathbf{r}) + \sum_{w_s=1}^{n_{w_s}} u_{w_s} \Phi_{w_s}(\mathbf{r}), \tag{9}$$

with $n_w = n_{w_r} + n_{w_s}$. The wave functions are defined as:

$$\Phi_w(\mathbf{r}\,(x,y)) = \begin{cases} \Phi_{w_r}(x,y) = \{\sin(k_{xw_r}x), \cos(k_{xw_r}x)\}\ e^{-jk_{yw_r}y} \\ \Phi_{w_s}(x,y) = e^{-jk_{xw_s}x}\ \{\sin(k_{yw_s}y), \cos(k_{yw_s}y)\} \end{cases} \tag{10}$$

where $\{f(x,y), g(x,y)\}\, h(x,y)$ indicates the definition of two independent basis functions $f(x,y).h(x,y)$ and $g(x,y).h(x,y)$. The only requirement for these wave functions to be exact solutions of the Helmholtz equation (6) is that the wave number components in (10) have to satisfy:

$$(k_{xw_r})^2 + (k_{yw_r})^2 = (k_{xw_s})^2 + (k_{yw_s})^2 = k_j^2. \tag{11}$$

Desmet [7] proposes to select the following wave number components:

$$(k_{xw_r}, k_{yw_r}) = \left(\frac{w_1 \pi}{L_x}, \pm\sqrt{k_j^2 - (k_{xw_r})^2} \right), \quad w_1 = 0, 1, 2, \ldots \tag{12}$$

$$(k_{xw_s}, k_{yw_s}) = \left(\pm\sqrt{k_j^2 - (k_{yw_s})^2}, \frac{w_2 \pi}{L_y} \right), \quad w_2 = 0, 1, 2, \ldots \tag{13}$$

The dimensions L_x and L_y are the dimensions of the (preferably smallest) bounding rectangle circumscribing the problem domain. This infinite set of wave functions has to be truncated into a finite set. The upper limit $w_\bullet$ in the wave number selection (12)-(13) is chosen accordingly to the following truncation rule:

$$\frac{w_\bullet \pi}{L_\bullet} \geqslant T \max_j (k_j). \tag{14}$$

The physical wavenumber k_j corresponds to the largest physical wavenumber in the problem domain. T is a user defined truncation factor.

3.2.3 Wave based model construction

Within the problem domain, the proposed solution expansion (9) always exactly satisfies the Helmholtz equation(s) (6), irrespective of the values of the unknown contribution factors u_w. These functions may however violate the imposed boundary and interface conditions. The errors on the boundaries and interfaces are minimized in an integral sense using a Galerkin weighted residual formulation. This yields an algebraic equation linking the unknown wave function contribution factors. The enforcement that this equation should hold for any combination of the weighting function results in a matrix system of equations, which can be solved for the contribution factors of each wave function in the problem domain.

3.2.4 Solution of the system of equations and postprocessing

The fourth step in the WB modeling process is the solution of the matrix equation. The back substitution of the wave function contribution factors into the field variable expansions (8), yields an approximation $\hat{u}_j(\mathbf{r})$ of the dynamic field variables. Also higher-order variables can easily be obtained by applying the corresponding differential operator to the wave function expansion.

3.3 WBM applied to poroelastic problems

To apply the WB theory to poroelastic materials, the Biot equations have to be decoupled into a set of Helmholtz equations. In the case that the material is isotropic, a possible decomposition for the solid displacements is given by:

$$\left\{ \begin{array}{c} u_x^s(\mathbf{r}) \\ u_y^s(\mathbf{r}) \end{array} \right\} = \nabla(-\frac{1}{k_{l_1}^2} e_1^s(\mathbf{r}) - \frac{1}{k_{l_2}^2} e_2^s(\mathbf{r})) + \nabla \times \frac{1}{k_t^2} \omega^s(\mathbf{r}) \tag{15}$$

with $e_1^s(\mathbf{r})$ and $e_2^s(\mathbf{r})$ two volumetric strains ($e^s(\mathbf{r}) = e_1^s(\mathbf{r}) + e_2^s(\mathbf{r})$) and $\omega^s(\mathbf{r})$ the rotational strain of the solid phase. By substituting (15) in the Biot equations (1), one obtains the following set of three decoupled Helmholtz equations:

$$\nabla^4 e^s(\mathbf{r}) + A_1 \nabla^2 e^s(\mathbf{r}) + A_2 e^s(\mathbf{r}) = (\nabla^2 e_1^s(\mathbf{r}) + k_{l_1}^2 e_1^s(\mathbf{r}))(\nabla^2 e_2^s(\mathbf{r}) + k_{l_2}^2 e_2^s(\mathbf{r})) = 0 \tag{16}$$

$$\nabla^2 \omega^s(\mathbf{r}) + k_t^2 \omega^s(\mathbf{r}) = 0 \tag{17}$$

Equation (16) indicates the existence of two compressional wave types with wave numbers k_{l_1} and k_{l_2},

$$\begin{cases} k_{l_1} = \sqrt{\frac{A_1}{2} - \sqrt{\frac{A_1^2}{4} - A_2}} \\ k_{l_2} = \sqrt{\frac{A_1}{2} + \sqrt{\frac{A_1^2}{4} - A_2}} \end{cases} \quad \text{with} \quad \begin{cases} A_1 = \omega^2 \frac{\rho_{11}^* R - 2\rho_{12}^* Q + \rho_{22}^* (\lambda + 2N + \frac{Q^2}{R})}{(\lambda + 2N + \frac{Q^2}{R})R - Q^2} \\ A_2 = \omega^4 \frac{\rho_{11}^* \rho_{22}^* - (\rho_{12}^*)^2}{(\lambda + 2N + \frac{Q^2}{R})R - Q^2} \end{cases} \tag{18}$$

and equation (17) indicates the existence of one shear wave type with wave number k_t:

$$k_t = \omega \sqrt{\frac{\rho_{11}^* \rho_{22}^* - (\rho_{12}^*)^2}{N \rho_{22}^*}} \tag{19}$$

The above discussion indicates that the mathematical description of a poroelastic problem results in a system of three Helmholtz equations (6) with:

- N_H=3
- $u_1(\mathbf{r}) = e_1^s(\mathbf{r})$, $u_2(\mathbf{r}) = e_2^s(\mathbf{r})$, $u_3(\mathbf{r}) = \omega^s(\mathbf{r})$
- $k_1 = k_{l_1}$, $k_2 = k_{l_1}$, $k_3 = k_t$
- $\mathcal{F}_j(\mathbf{r}) = 0$

According to the WB principles as explained in section 3, each of the three dynamic variables in the decoupled Biot equations, $e_1^s(\mathbf{r})$, $e_2^s(\mathbf{r})$ and $\omega^s(\mathbf{r})$, is approximated by a solution expansion of form (8). Since the three Helmholtz equations (16) are homogeneous, no particular solutions have to be defined. For the selection of the wave number components in the solution expansion of each dynamic variable, the corresponding wave numbers k_{l_1}, k_{l_2} and k_t are taken into account.

Each field variable a can be written in function of the strain fields by applying a corresponding differential operator:

$$a = \mathcal{L}_a \begin{bmatrix} e_1^s(\mathbf{r}) \\ e_2^s(\mathbf{r}) \\ \omega^s(\mathbf{r}) \end{bmatrix} \tag{20}$$

The differential operators for the normal and tangential displacements and the stresses in both phases are defined as follows:

$$\mathcal{L}_{u_n^s} = \begin{bmatrix} -\frac{1}{k_{l_1}^2}\frac{\partial}{\partial \gamma_n} & -\frac{1}{k_{l_2}^2}\frac{\partial}{\partial \gamma_n} & +\frac{1}{k_t^2}\frac{\partial}{\partial \gamma_s} \end{bmatrix} \tag{21}$$

$$\mathcal{L}_{u_s^s} = \begin{bmatrix} -\frac{1}{k_{l_1}^2}\frac{\partial}{\partial \gamma_s} & -\frac{1}{k_{l_2}^2}\frac{\partial}{\partial \gamma_s} & -\frac{1}{k_t^2}\frac{\partial}{\partial \gamma_n} \end{bmatrix} \tag{22}$$

$$\mathcal{L}_{u_n^f} = \begin{bmatrix} -\frac{\mu_{k_{l_1}}}{k_{l_1}^2}\frac{\partial}{\partial \gamma_n} & -\frac{\mu_{k_{l_1}}}{k_{l_2}^2}\frac{\partial}{\partial \gamma_n} & +\frac{\mu_{k_t}}{k_t^2}\frac{\partial}{\partial \gamma_s} \end{bmatrix} \tag{23}$$

$$\mathcal{L}_{\sigma_n^s} = \begin{bmatrix} -\frac{2N}{k_{l_1}^2}\frac{\partial^2}{\partial \gamma_n^2} + \lambda + \frac{Q^2}{R} + \mu_{k_{l_1}} Q & -\frac{2N}{k_{l_2}^2}\frac{\partial^2}{\partial \gamma_n^2} + \lambda + \frac{Q^2}{R} + \mu_{k_{l_2}} Q & \frac{2N}{k_t^2}\frac{\partial^2}{\partial \gamma_n \partial \gamma_s} \end{bmatrix} \tag{24}$$

$$\mathcal{L}_{\sigma_s^s} = \begin{bmatrix} -\frac{2N}{k_{l_1}^2}\frac{\partial^2}{\partial \gamma_n \partial \gamma_s} & -\frac{2N}{k_{l_2}^2}\frac{\partial^2}{\partial \gamma_n \gamma_s} & \frac{N}{k_t^2}(\frac{\partial^2}{\partial \gamma_s^2} - \frac{\partial^2}{\partial \gamma_n^2}) \end{bmatrix} \tag{25}$$

$$\mathcal{L}_{\sigma^f} = \begin{bmatrix} Q + \mu_{k_{l_1}} R & Q + \mu_{k_{l_2}} R & 0 \end{bmatrix} \tag{26}$$

$\mu_{k_{l_1}}$, $\mu_{k_{l_2}}$ and μ_{k_t} are the ratios of the fluid and the solid displacements of the different wave types and are defined by Allard [2]. $\gamma_\mathbf{s}$ is the tangential direction of the boundary.

The boundary residuals of the porous material can be determined using the same differential operators. The mutual coupling between the three wave field components is entirely contained within the boundary and continuity conditions specified along the boundaries and interfaces. For a full description of the WBM for uncoupled poroelastic materials, which also includes a decoupling of the Biot equations based on scalar and vector potentials and a description of the continuity conditions between two poroelastic subdomains, the reader is referred to [10].

4 Stress singularities

This paper focusses on the existence and treatment of stress singularities in poroelastic materials. As indicated by Sinclair [14], infinite values of stresses are physically impossible, but indicate that no finite stresses can be computed by the linear theory of elasticity. Generally, two classes of stress singularities are distinguished. The first class originates from concentrated loads applied over regions with a vanishingly small area. In the second class, singularities occur away from concentrated loads and always in concert with discontinuities. It is this class that will be considered in this paper. For a polygonal plate domain, discontinuity singularities can be expected at the corner points. Typically, this kind of singularity arises when the internal angle formed by the two sides of a corner exceeds a critical value, which depends on the imposed boundary conditions. As indicated by Vanmaele et al. [11, 12], the WBM suffers from convergence problems when stress singularities are present. These problems arise from the global character of the wave functions, which have difficulties with capturing the singular behavior in the corner. As can be expected, the same kind of problems appear when stress singularities are present in corners of poroelastic problem domains. The objective of this section is to find analytical solutions that accurately describe the displacement and stress fields in the vicinity of corners with a singularity. In this way, criteria can be defined to determine whether stress singularities are present. If so, the set of wave functions can be extended with additional enrichment functions which accurately represent the singular behavior close to the corner point.
To find an analytical solution that asymptotically approximates the displacement and stress fields in a corner of a poroelastic problem domain, some assumptions are made:

- The stresses in the vicinity of the corner point are hardly affected by the boundary conditions away from the considered corner point.
- Only homogeneous boundary conditions are considered, the imposed values of the prescribed stresses or displacements are zero.
- Only wedges consisting of a single poroelastic material are considered.

Under these assumptions it is appropriate to study an infinite wedge domain as shown in figure 1. The solution of this infinite wedge domain only exactly represents the dynamic fields in the domain in the case that the edges extend to infinity. However, they present a very good approximation for the actual behavior in the vicinity of the corner of a finite domain as long as the same radial boundary conditions are imposed as for the actual problem. Following the methodology of Sinclair [15], polar cylindrical coordinates r and θ are employed and the open angular region of interest $\mathcal{R}$ is given by:

$$\mathcal{R} = \{(r,\theta)|\ 0 < r < \infty,\ -\frac{\alpha}{2} < \theta < \frac{\alpha}{2}\} \tag{27}$$

The analytical solution needs to satisfy:

1. The Biot equations
2. The imposed boundary conditions
3. The regularity requirements at the vertex

Starting from the analytical solution for the strain fields, the stresses and their singular behavior can be evaluated.

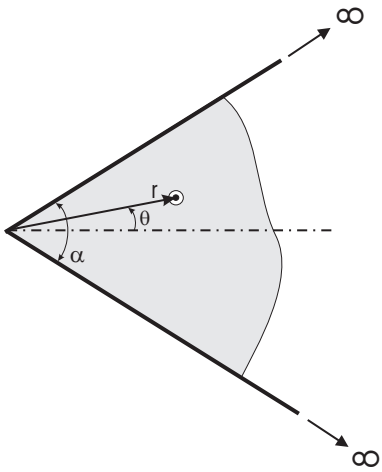

Figure 1: 2D infinite poroelastic wedge domain

4.1 Analytical solution for an infinite wedge

The solution for the displacement and the stress fields is defined starting from the decoupled Biot equations (16)-(17). Assuming a separable function for the strains $e_1^s(r,\theta)$, $e_2^s(r,\theta)$ and $\omega^s(r,\theta)$ in polar coordinates leads to the following homogenous solution [16]:

$$e_1^s(\mathbf{r}) = \sum_{b=1}^{\infty}[\cos(\lambda_{l_1 b}\theta)R_{\lambda_{l_1 b}}(k_{l_1}r) + \sin(\lambda^*_{l_1 b}\theta)R_{\lambda^*_{l_1 b}}(k_{l_1}r)] \tag{28}$$

$$e_2^s(\mathbf{r}) = \sum_{b=1}^{\infty}[\cos(\lambda_{l_2 b}\theta)R_{\lambda_{l_2 b}}(k_{l_2}r) + \sin(\lambda^*_{l_2 b}\theta)R_{\lambda^*_{l_2 b}}(k_{l_2}r)] \tag{29}$$

$$\omega^s(\mathbf{r}) = \sum_{b=1}^{\infty}[\cos(\lambda_{tb}\theta)R_{\lambda_{tb}}(k_t r) + \sin(\lambda^*_{tb}\theta)R_{\lambda^*_{tb}}(k_t r)] \tag{30}$$

where

$$R_\lambda(z) = A_\lambda J_\lambda(z) + B_\lambda Y_\lambda(z). \tag{31}$$

A_λ and B_λ are constants of integration and $J_\lambda(z)$ and $Y_\lambda(z)$ are respectively the ordinary and modified Bessel functions of the first kind. $\lambda_\bullet$ indicate the eigenvalues associated with symmetric eigenfunctions with respect to the axis $\theta = 0$ and the eigenvalues $\lambda^*_\bullet$ are associated with anti-symmetric eigenfunctions. This paper uses the following shortened notations:

$$\lambda_{l_1} = \lambda_{l_1 b} \text{ or } \lambda^*_{l_1 b} \tag{32}$$

$$\lambda_{l_2} = \lambda_{l_2 b} \text{ or } \lambda^*_{l_2 b} \tag{33}$$

$$\lambda_t = \lambda_{tb} \text{ or } \lambda^*_{tb} \tag{34}$$

depending on whether they are associated with symmetric or anti-symmetric eigenfunctions. The application of the boundary conditions at $\theta = \pm\alpha/2$ leads to a system of equations which can be solved for the unknown integration constants:

$$[\mathbf{A}]\{\mathbf{c}\} = \mathbf{0} \tag{35}$$

with $[\mathbf{A}]$ the coefficient matrix and $\{\mathbf{c}\}$ the vector of unknown constants of integration. Since trivial solutions should be eliminated, the determinant of the coefficient matrix must be zero:

$$\det[\mathbf{A}] = 0 \tag{36}$$

and the eigenvalues $\lambda_{l_1 b}$, $\lambda^*_{l_1 b}$, $\lambda_{l_2 b}$, $\lambda^*_{l_2 b}$, λ_{tb}, λ^*_{tb} are the solutions of this characteristic equation. Since it is assumed that the boundary conditions at infinity have no influence on the singular behavior at the corner,

they are discarded. This may lead to solutions of (35) which are non-unique. For our objective, this is not a problem, since we are only interested in possible distributions of the different fields in the vicinity of the corner.

At the corner point, the regularity requirements still have to be fulfilled. Consistent with [15], the following conditions have to be imposed at the tip of corner (r=0):

$$u_r^s(0,\theta) = \text{finite} \tag{37}$$
$$u_\theta^s(0,\theta) = \text{finite} \tag{38}$$
$$u_r^f(0,\theta) = \text{finite} \tag{39}$$

Applying equation (15) in polar coordinates leads to:

$$u_r^s(r,\theta) = -\frac{1}{k_{l_1}^2}\frac{\partial e_1^s}{\partial r} - \frac{1}{k_{l_2}^2}\frac{\partial e_2^s}{\partial r} + \frac{1}{k_t^2 r}\frac{\partial \omega^s}{\partial \theta} \tag{40}$$
$$u_r^f(r,\theta) = -\frac{\mu_{k_{l_1}}}{k_{l_1}^2}\frac{\partial e_1^s}{\partial r} - \frac{\mu_{k_{l_2}}}{k_{l_2}^2}\frac{\partial e_2^s}{\partial r} + \frac{\mu_{k_t}}{k_t^2 r}\frac{\partial \omega^s}{\partial \theta} \tag{41}$$
$$u_\theta^s(r,\theta) = -\frac{1}{k_{l_1}^2}\frac{1}{r}\frac{\partial e_1^s}{\partial \theta} - \frac{1}{k_{l_2}^2}\frac{1}{r}\frac{\partial e_2^s}{\partial \theta} - \frac{1}{k_t^2}\frac{\partial \omega^s}{\partial r} \tag{42}$$

These expressions have to remain finite when $r \to 0$. Since (40) and (41) depend on the same derivatives and only differ in some constant scaling factors, both are leading to the same conditions. Introduction of the homogenous solutions (28)-(30) in expressions (40) and (42) leads to the following conditions for the possible displacement fields:

$$\begin{aligned} u_r^s(r,\theta)|_{r=0} = \lim_{r\to 0} \Big[& c_1(\theta) \Big[A_{\lambda_{l_1}} \Big(J_{\lambda_{l_1}-1}(k_{l_1} r) - J_{\lambda_{l_1}+1}(k_{l_1} r) \Big) \\ & + B_{\lambda_{l_1}} \Big(Y_{\lambda_{l_1}-1}(k_{l_1} r) - Y_{\lambda_{l_1}+1}(k_{l_1} r) \Big) \Big] \\ & + c_2(\theta) \Big[A_{\lambda_{l_2}} \Big(J_{\lambda_{l_2}-1}(k_{l_2} r) - J_{\lambda_{l_2}+1}(k_{l_2} r) \Big) \\ & + B_{\lambda_{l_2}} \Big(Y_{\lambda_{l_2}-1}(k_{l_2} r) - Y_{\lambda_{l_2}+1}(k_{l_2} r) \Big) \Big] \\ & + \frac{c_3(\theta)}{r} \left[A_{\lambda_t} J_{\lambda_t}(k_t r) + B_{\lambda_t} Y_{\lambda_t^*}(k_t r) \right] \Big] = \text{finite} \end{aligned} \tag{43}$$

$$\begin{aligned} u_\theta^s(r,\theta)|_{r=0} = \lim_{r\to 0} \Big[& \frac{c_4(\theta)}{r} \Big[A_{\lambda_{l_1}} J_{\lambda_{l_1}}(k_{l_1} r) + B_{\lambda_1} Y_{\lambda_{l_1}^*}(k_{l_1} r) \Big] \\ & + \frac{c_5(\theta)}{r} \Big[A_{\lambda_{l_2}} J_{\lambda_{l_2}}(k_{l_2} r) + B_{\lambda_2} Y_{\lambda_{l_2}^*}(k_{l_2} r) \Big] \\ & + c_6(\theta) \Big[A_{\lambda_{l_1}} \left(J_{\lambda_t - 1}(k_t r) - J_{\lambda_t+1}(k_t r) \right) \\ & + B_{\lambda_t} \left(Y_{\lambda_t-1}(k_t r) - Y_{\lambda_t+1}(k_t r) \right) \Big] \Big] = \text{finite} \end{aligned} \tag{44}$$

with $c_\bullet(\theta)$ a function that only depends on coordinate θ. Since

$$\lim_{r\to 0} Y_\lambda(z) = -\infty \tag{45}$$

all the integration constants B_λ have to be zero to fulfill the regularity conditions. Since Bessel functions of the first kind can be expanded using a power series [17]:

$$J_\lambda(z) = \sum_{k=0}^{\infty} \frac{(-1)^k}{k!\Gamma(\lambda + k + 1)} \frac{z^{2k+\lambda}}{2} \tag{46}$$

the remaining expressions stay finite if all the eigenvalues are larger than 1. Taking this into account, the eigenfunctions become:

$$R_{\lambda_{l_1}} = A_{\lambda_{l_1}} J_{\lambda_{l_1}}(k_{l_1} r) \qquad \lambda_{l_1} > 1 \tag{47}$$

$$R_{\lambda_{l_2}} = A_{\lambda_{l_2}} J_{\lambda_{l_2}}(k_{l_2} r) \qquad \lambda_{l_2} > 1 \tag{48}$$

$$R_{\lambda_t} = A_{\lambda_t} J_{\lambda_t}(k_t r) \qquad \lambda_t > 1 \tag{49}$$

4.2 The strain and stress fields in the vicinity of the corner

This paragraph investigates when stress singularities are present. Starting from the analytical solution for the displacement fields, admissible strain and stress fields can be determined in the vicinity of the corner. The strains can be written as:

$$e_r^\bullet(r,\theta) = \frac{\partial u_r^\bullet(r,\theta)}{\partial r} \tag{50}$$

$$e_\theta^\bullet(r,\theta) = \frac{1}{r}\frac{\partial u_\theta^\bullet(r,\theta)}{\partial \theta} + \frac{u_r^\bullet(r,\theta)}{r} \tag{51}$$

$$e_{r\theta}^\bullet(r,\theta) = \frac{1}{r}\frac{\partial u_r^\bullet(r,\theta)}{\partial \theta} + \frac{\partial u_\theta^\bullet(r,\theta)}{\partial r} - \frac{u_\theta^\bullet(r,\theta)}{r} \tag{52}$$

The stresses in both phases of the isotropic material, expressed in cylindrical coordinates, are given by:

$$\sigma_r^s(r,\theta) = (\lambda + \frac{Q^2}{R})e^s(r,\theta) + Qe^f(r,\theta)) + 2Ne_r^s(r,\theta) \tag{53}$$

$$\sigma_\theta^s(r,\theta) = (\lambda + \frac{Q^2}{R})e^s(r,\theta) + Qe^f(r,\theta) + 2Ne_\theta^s(r,\theta) \tag{54}$$

$$\sigma_{r\theta}^s(r,\theta) = Ne_{r\theta}^s(r,\theta) \tag{55}$$

$$\sigma^f(r,\theta) = Qe^s(r,\theta) + Re^f(r,\theta) \tag{56}$$

In this way, the possible stress distributions in the vicinity of the corner can be expressed in function of the admissible longitudinal and rotational strain fields (28)-(30), taking into account the eigenfunctions (47)-(49). Since the longitudinal strains $e_1^s(r,\theta)$ and $e_2^s(r,\theta)$ do not give rise to an unbounded value if $r \to 0$ the stresses in the fluid phase will always remain finite. However, singularities will exist in the solid phase if $e_r^s(r,\theta)$, $e_\theta^s(r,\theta)$ or $e_{r\theta}^s(r,\theta)$ becomes singular when $r \to 0$. Substituting the expressions of the admissible displacement fields in the expressions of the strains (50)-(52) and using the power series expansion for the Bessel function of the first kind (46), it can easily be verified when singularities can exist. For example the possible fields for the radial strain $e_r^s(r,\theta)$ are given by:

$$\begin{aligned}
e_r^s(r,\theta) = &-\frac{1}{4}\Big[A_{\lambda_{l_1 b}}\cos(\lambda_{l_1 b}\theta)\Big(J_{\lambda_{l_1 b}-2}(k_{l_1}r) - 2J_{\lambda_{l_1 b}}(k_{l_1}r) + J_{\lambda_{l_1 b}+2}(k_{l_1}r)\Big) \\
&\quad + A_{\lambda_{l_1^* b}}\sin(\lambda^*_{l_1 b}\theta)\Big(J_{\lambda_{l_1^* b}-2}(k_{l_1}r) - 2J_{\lambda_{l_1^* b}}(k_{l_1}r) + J_{\lambda^*_{l_1 b}+2}(k_{l_1}r)\Big)\Big] \\
&-\frac{1}{4}\Big[A_{\lambda_{l_2 b}}\cos(\lambda_{l_2 b}\theta)\Big(J_{\lambda_{l_2 b}-2}(k_{l_2}r) - 2J_{\lambda_{l_2 b}}(k_{l_2}r) + J_{\lambda_{l_2 b}+2}(k_{l_2}r)\Big) \\
&\quad + A_{\lambda_{l_2^* b}}\sin(\lambda^*_{l_2 b}\theta)\Big(J_{\lambda^*_{l_2 b}-2}(k_{l_2}r) - 2J_{\lambda^*_{l_2 b}}(k_{l_2}r) + J_{\lambda^*_{l_2 b}+2}(k_{l_2}r)\Big)\Big] \\
&\quad - \frac{1}{k_t^2 r^2}\Big[-A_{\lambda_{tb}}\lambda_{tb}\sin(\lambda_{tb}\theta)J_{\lambda_{tb}}(k_t r) + A_{\lambda^*_{tb}}\lambda^*_{tb}\cos(\lambda^*_{tb}\theta)J_{\lambda^*_{tb}}(k_t r)\Big] \\
&\quad + \frac{1}{2k_t r}\Big[-A_{\lambda_{tb}}\lambda_{tb}\sin(\lambda_{tb}\theta)(J_{\lambda_{tb}-1}(k_t r) - J_{\lambda_{tb}+1}(k_t r)) \\
&\qquad + A_{\lambda^*_{tb}}\lambda^*_{tb}\cos(\lambda^*_{tb}\theta)(J_{\lambda^*_{tb}-1}(k_t r) - J_{\lambda^*_{tb}+1}(k_t r))\Big]
\end{aligned} \tag{57}$$

When substituting the Bessel functions by their series expansion it is clear that the stress field $\sigma_r^s(r,\theta)$ becomes singular in the corner point if one of the eigenvalues becomes smaller than 2. The order of the singularity is $\lambda - 2$. Singularities in the other stress components of the solid phase can be studied by writing down similar expressions for $e_\theta^s(r,\theta)$ and $e_{r\theta}^s(r,\theta)$. The order of these singularities is also $\lambda - 2$.

4.3 Analytical solution for the sliding edge infinite wedge

This paragraph studies the specific case of an infinite wedge with imposed sliding edge conditions on both edges and searches for the analytical solution by determining the required eigenvalues. The boundary conditions, expressed in polar coordinates, are:

$$u_\theta^s(r,\pm\frac{\alpha}{2}) = 0, \tag{58}$$

$$u_\theta^f(r,\pm\frac{\alpha}{2}) = 0, \tag{59}$$

$$\sigma_{r\theta}^s(r,\pm\frac{\alpha}{2}) = 0. \tag{60}$$

These six boundary conditions are applied to the homogenous solution expansions. The solution of the resulting characteristic equation leads to the following set of eigenvalues:

$$\lambda_{l_1 b} = \frac{2b\pi}{\alpha} \qquad \lambda_{l_2 b} = \frac{2b\pi}{\alpha} \qquad \lambda_{tb} = (2b-1)\frac{\pi}{\alpha} \tag{61}$$

$$\lambda_{l_1 b}^* = (2b-1)\frac{\pi}{\alpha} \qquad \lambda_{l_2 b}^* = (2b-1)\frac{\pi}{\alpha} \qquad \lambda_{tb}^* = \frac{2b\pi}{\alpha} \tag{62}$$

with b=1,2,.... The homogenous solutions, using the eigenfunctions (47)-(49) and the above defined eigenvalues form exact analytical solutions of the infinite wedge domain since they fulfill the boundary conditions, the decoupled Biot equations and the regularity conditions. Stress singularities are present if at least one of the eigenvalues is smaller than 2. For a corner with two sliding edges, this is true if the angle α exceeds the critical value $\pi/2$.
In case a singularity is present in the corner, the corresponding homogenous solutions with eigenvalues < 2 will be added to the regular wave function sets. Since they accurately represent the singularity in the vicinity of the considered corner, this addition will lead to better convergence properties as will be shown in a validation study.

4.4 Other radial boundary conditions

It can be easily verified that it is impossible to find an exact dynamic solution in case other radial boundary conditions are imposed. This is similar as compared to plate bending and plate membrane problems. Also, in the case of poroelastic materials the eigenvalues can not be deduced from the radial boundary conditions. Vanmaele [11, 12] proposes to start from the analytical solutions for static problems. These solutions do not form exact solutions of the dynamic problem and can as such not be incorporated in the WBM. The static solutions are only used to define static eigenvalues from which the dynamic ones can be derived. For poroelastic materials, static solutions of an infinite wedge to study singularities are not yet defined in literature. This topic will be dealt with in the future.

5 Validation example

This section demonstrates the computational efficiency of the WBM as compared to the FEM in the case that stress singularities are present. Firstly, the presence of stress singularities is studied, validating the criteria developed theoretically in the previous section and indicating the problems arising when no special purpose

functions are included. Next, the singularity theory is incorporated in the WBM. The special purpose enrichment functions are discussed and the performance of the classical and enriched WB predictions are compared with FE results, both concerning accuracy and calculation time. All WB routines are implemented in Matlab R2009. The FE predictions are obtained using Comsol 3.5a. The FE model uses a ($\mathbf{u^s}$,$\mathbf{u^f}$)-formulation and includes four degrees of freedom per node for the poroelastic domain. Cubic Lagrangian triangular finite elements are used. The FE models are solved using a direct UMFPACK solver. The mentioned calculation times include both the construction and the solution times since the models are frequency dependent. All calculations are performed on a intel Xeon 5540 based system (2.53GHz) with a 24 GB memory running a linux operating system.

5.1 Existence of stress singularities and impact on WB accuracy

To verify the existence of stress singularities, a poroelastic problem domain is considered, shown in figure 2. It consists of a polygonal poroelastic domain containing a polyurethane foam saturated with air. The material properties are given in table 1. Boundaries Γ_1, Γ_2 and Γ_3 are sliding edge boundaries, see equation (5). On Γ_4 a normal stress resultant of $1N/m^2$ is imposed.

Air data	Porous material data
k=2.57·10^{-2}W/(mK)	E_s=70·10^{3}Pa
c_p=1.005·10^{3}J/(kgK)	η_l=0.265
R^{gas}=286.7m^2/(s^{2}K)	ν=0.39
T=293.15K	ρ_s=22.1kg/m^3
γ=1.4	ϕ=0.98
ν_f=15.11·10^{-6}m^2/s	Λ=1.1·10^{-4}
ρ_f=1.205kg/m^3	Λ'=7.42·10^{-4}
	σ_{res}=3.75·10^{3}kg/(m^{3}s)
	α_∞=1.17

Table 1: Material data

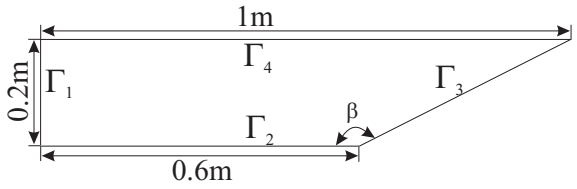

Figure 2: Problem geometry of a trapezoid poroelastic domain

As predicted in section 4.3, stress singularities are present in a corner with imposed sliding edge conditions on both edges if the internal angle is larger than $\pi/2$. As shown in a previous paper [10], which contains a rectangular poroelastic domain with sliding edge conditions, no stress singularities are present. Application of the singularity theory to the problem geometry described above, predicts that this problem configuration does contain a singularity. This is validated by means of a FE calculation at 200Hz. The FE model of the problem geometry contains 124000 dofs. Nine adaptive mesh refinements are performed, based on a L_2-norm of the error, to obtain accurate models. Figure 3 shows the stress field σ^s_{xy} obtained with the FEM, indicating a very steep gradient at the bottom of the poroelastic subdomain with a maximum of $\sim 18.6N/m^2$ in the corner point, indicating that a stress singularity is present. The stresses away from the corner point stay well below $0.5N/m^2$.

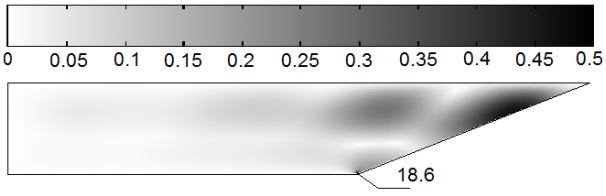

Figure 3: Contour plot of $\sigma^s_{xy}(x,y)$ [N/m^2] in the poroelastic domain, obtained with the FEM at 200Hz

A WB model is constructed for the problem geomety to verify whether stress singularities have a negative influence on the accuracy of the WBM. A truncation factor, $T = 1.5$, is applied to the wave type with the largest wave number and the number of wave functions of the other wave types are scaled such that each wave function expansion exhibits a similar spatial resolution. The FE models serve as a reference and are constructed based on 6 adaptive refinements for each frequency. Figure 4 shows the frequency response

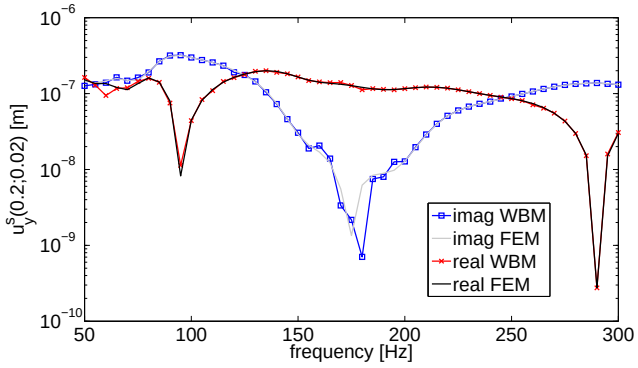

Figure 4: Frequency response function of $u_y^s(0.2, 0.02)$ obtained with the WBM

functions of u_y^s in a point (0.2,0.02) of the poroelastic domains. The accuracy is clearly affected by the presence of the singularity.

5.2 Validation of the Wave Based Method with special purpose enrichment functions

This paragraph shows the beneficial effect of incorporating special purpose enrichment functions in the WBM. These functions will shortly be called 'corner functions' in this validation example and the use of the WBM with corner functions is indicated in graphs by WBM CF. The WBM, the WBM CF and the FEM results are compared based on both accuracy and computational effort.

5.2.1 WBM CF

The eigenvalues of the characteristic equation (36) for the combination of two boundaries with imposed sliding edge conditions lead to eigenvalues given by the expressions (61)-(62). Singularities are present if $\lambda < 2$. Only the eigenfunctions associated with eigenvalues < 2 are added to the wave function set. Since the internal angle β is $153.4°$, these eigenvalues are:

$$\lambda_{l_1}^* = \lambda_{l_2}^* = \lambda_t = \frac{\pi}{\alpha} = 1.173 = \lambda_{CF} \tag{63}$$

and the corresponding corner functions, added to the corresponding wave function sets for respectively $e_1^s(\mathbf{r})$, $e_2^s(\mathbf{r})$ and $\omega^s(\mathbf{r})$ are:

$$\Phi_{l_1}^{CF} = \sin(\lambda_{CF}\theta) J_{\lambda_{CF}}(k_{l_1} r) \tag{64}$$

$$\Phi_{l_2}^{CF} = \sin(\lambda_{CF}\theta) J_{\lambda_{CF}}(k_{l_2} r) \tag{65}$$

$$\Phi_{t}^{CF} = \cos(\lambda_{CF}\theta) J_{\lambda_{CF}}(k_{t} r) \tag{66}$$

Compared the WBM, the WBM CF has three more functions in its expansion sets.

5.2.2 Comparison of WBM and WBM CF

A first indication of the difference in accuracy between the WBM and the WBM CF is given by a comparison of contour plots of the stress fields in the poroelastic domain. The calculations are performed at 200 Hz with a truncation factor of $T = 2$ leading to 200 compressional wave functions for the strain expansion e_1^s, 460 compressional wave functions for the strain expansion e_2^s and 84 shear wave functions. The WB CF model contains the same number of wave functions but is enriched with the three corner functions given above. Figure 5 compares the predicted stress fields $\sigma_{xy}^s(x, y)$ calculated with the WBM and the WBM CF. As

expected, the stress field peaks at the bottom corner. In order to more clearly illustrate the adverse effect of the singularity on the WB predictions in the whole poroelastic field, some contour lines are added to the figures. These lines clearly show the presence of spurious oscillations in the WBM prediction which do not appear when adding the three corner functions. In the WBM CF results, the stress field reaches ∞ at the corner point.

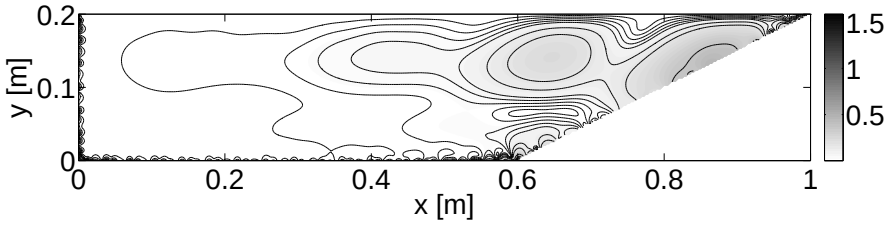

(a) WBM

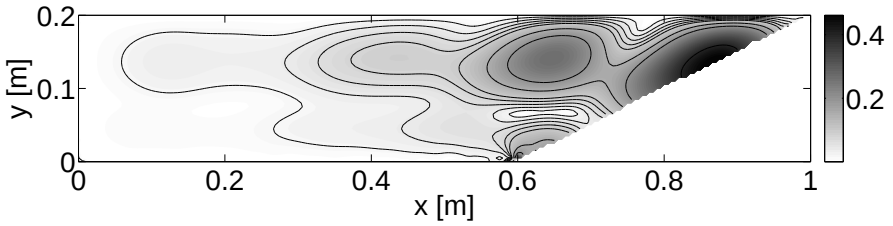

(b) WBM CF

Figure 5: Predicted stress field $\sigma^s_{xy}(x, y)[N/m^2]$ at 200 Hz

Figure 6 shows similar frequency response function to those presented in the previous paragraph, calculated with both the WBM and the WBM CF and compared to the FEM. These results confirm the increase in accuracy when corner functions are added.

5.3 Comparison of computational efficiency

Convergence curves at 200 Hz are calculated to demonstrate the beneficial convergence rate of the WBM CF as compared to both the WBM and the FEM. Fifteen FE models are constructed and are summarized in table 2. One additional adaptive refinement is performed between each two subsequent FEM models. The finest FE model in this table serves as reference calculation. The calculation time t_t is the total time needed to calculate the frequency dependent material properties, to construct and to solve the system matrices and to do

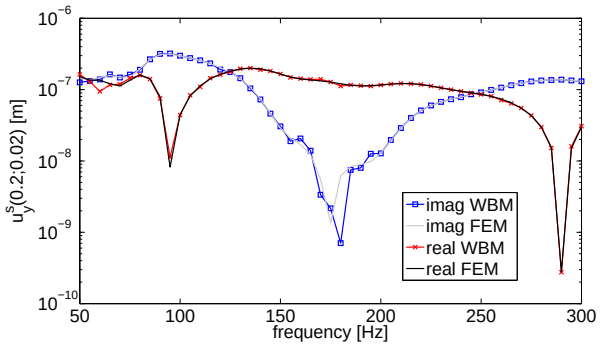

(a) WBM

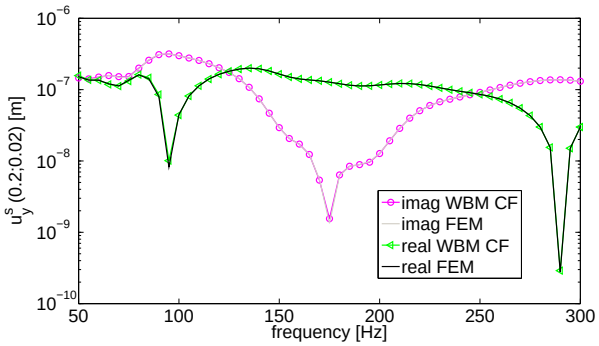

(b) WBM CF

Figure 6: Frequency response function of $u^s_y(0.2, 0.02)$ calculated with the WBM, the WBM CF and the FEM

the requested number of subsequent adaptive refinements. Different WB models are built with an increasing number of wave functions. The same truncation factor T is applied to the three different wave types and is increased for each sample. Tabel 3 shows the minimum and the maximum number of wave functions of each type at 200Hz. For the WBM CF the number of wave functions is increased with the three corner functions.

nr	♯ refs.	dofs	t_t [s]
1	0	316	0.98
2	1	676	1.09
3	2	1396	1.40
4	3	2572	1.67
5	4	5140	1.95
6	5	9532	2.90
7	6	18388	4.45
8	7	34300	7.75
9	8	66256	14.29
10	9	124000	28.11
11	10	244600	60.46
12	11	455908	134.26
13	12	896548	309.05
14	13	1696300	774.58
15	14	3238912	1942.19

Table 2: FE model data at 200Hz

	1^{st} dilat.	2^{nd} dilat.	rot.
min	28	16	56
max	856	376	2000

Table 3: WBM model data at 200Hz

To compare the convergence rate of the different methods, the relative prediction error $\langle\epsilon\rangle$ of a variable a is calculated as a function of CPU time. This prediction error is averaged over 26 response points which are equally distributed over the poroelastic domain:

$$\langle\epsilon\rangle = \frac{1}{26}\sum_{j=1}^{26}\epsilon_j \quad \text{with} \quad \epsilon_j = \frac{\|a(\mathbf{r_j}) - a^{ref}(\mathbf{r_j})\|}{\|a^{ref}(\mathbf{r_j})\|} \tag{67}$$

Figure 7 compares the convergence curves of the WBM, the WBM CF and the FEM at 200Hz for five poroelastic variables. The beneficial effect of adding corner functions to the wave function expansion is clearly illustrated. The accuracy increases and the convergence is stabilized. The WBM CF convergence curves show a steep decline and stabilize at a fixed prediction accuracy. This type of convergence behavior typically indicates that the model which is used as a reference has not yet converged to a better accuracy than the model with which it is compared. The WBM CF outperforms the FEM in efficiency: a better accuracy is obtained much less calculation time.

6 Conclusions

The WBM is a novel prediction technique which aims at relaxing the frequency limitations of element based techniques. Recently, the WBM has been applied to predict the dynamic behavior of poroelastic materials. This paper focuses on the existence of stress singularities, which can exist in the corners of poroelastic domains. Singularities are present if the corner angle exceeds a critical value, depending on the applied boundary conditions along the adjacent edges. If singularities are present, the accuracy of the WBM is clearly affected. This paper derives general criteria to determine whether stress singularities are present and proposes to use special purpose enrichment functions in the wave function expansion set to accurately capture this singular behavior. These so-called corner functions are exact solutions of the Biot equations and fulfill the boundary conditions and regularity conditions at the corner tip. Only for the special case of sliding edge boundary conditions, exact analytical solutions can be found. For this type of singularities, the effect of adding corner functions to the wave function expansion is validated. A numerical example verifies the advantageous effects on both the accuracy and the convergence speed of the method. The performance of the WBM with corner functions is also compared to that of the FEM, indicating a higher convergence rate and the potential of the WBM for poroelastic calculations.

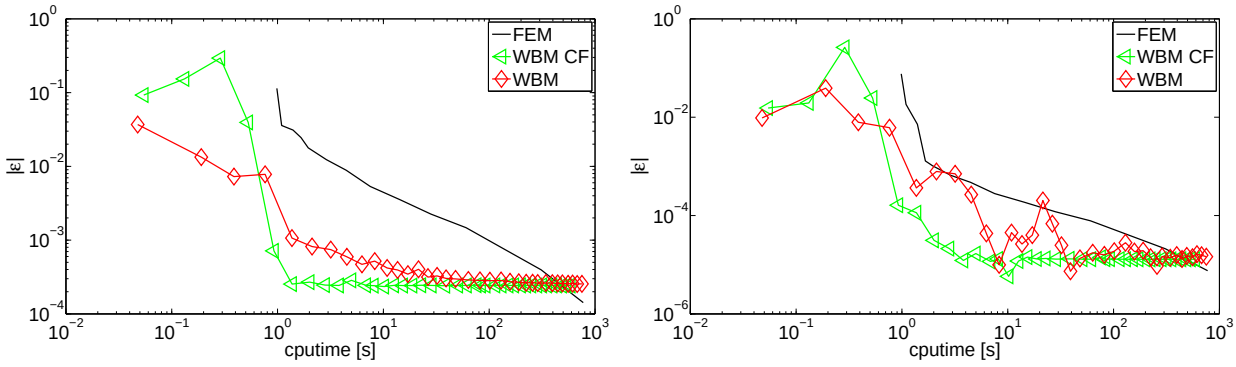

(a) $u_x^s(x,y)$

(b) $u_y^f(x,y)$

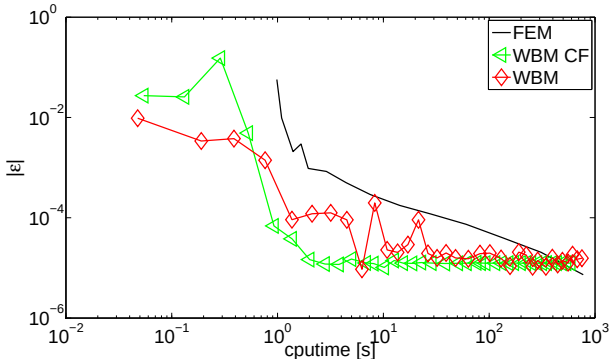

(c) $\sigma_x^s(x,y)$

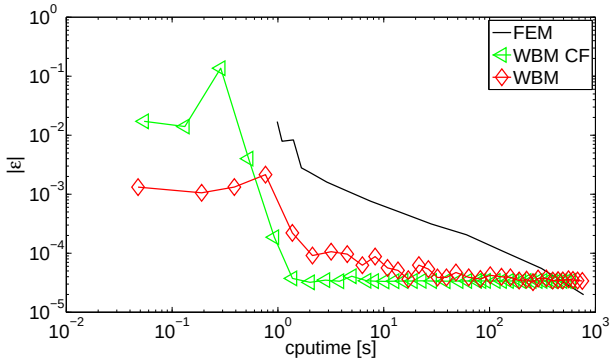

(d) $\sigma_y^s(x,y)$

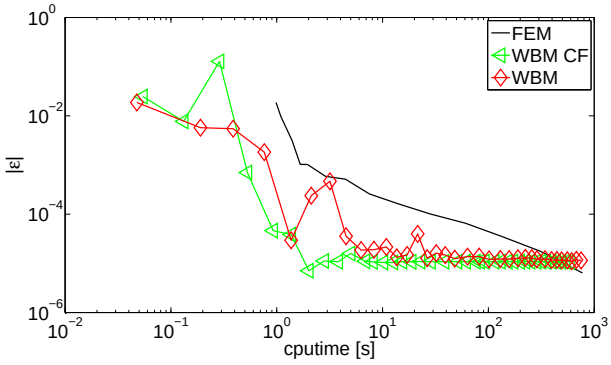

(e) $\sigma^f(x,y)$

Figure 7: Convergence curves at 200Hz for the WBM, the WBM CF and the FEM with FEM model number 9 as reference

Aknowledgements

Elke Deckers is a Doctoral Fellow of the Fund for Scientific Research-Flanders (F.W.O.), Belgium.

References

[1] M. A. Biot, *The theory of propagation of elastic waves in a fluid-saturated porous solid. I. Low frequency range. II. Higher frequency range*, Journal of the Acoustical Society of America, Vol. 28 (1956), pp. 168-191.

[2] J.-F. Allard, *Propagation of Sound in Porous Media: Modeling Sound Absorbing Materials*, Elsevier, New York (1998).

[3] N.-E. Hörlin, M. Nordström, P. Göransson, *A 3-D hierarchical FE formulation of Biot's equations for elasto-acoustic modelling of porous media*, Journal of Sound and Vibration, Vol. 245 (2001), pp. 633-652.

[4] O. Dazel, B. Brouard, C. Depollier, S. Griffiths, *An alternative Biot's displacement formulation for porous materials*, Journal of the Acoustical Society of America, Vol. 121 (2007), pp. 3509-3516.

[5] N. Atalla, R. Panneton, P. Debergue, *Enhanced weak integral formulation for the mixed ($\underline{u}$,$\underline{p}$) poroelastic equations*, Journal of the Acoustical Society of America, Vol. 109 (2001), pp. 3065-3068.

[6] N. Dauchez, S. Sahraoui, N. Atalla, *Convergence of poroelastic finite elements based on Biot displacement formulation*, Journal of the Acoustical Society of America, Vol. 109 (2001), pp. 33-40.

[7] W. Desmet, *A Wave Based prediction technique for coupled vibro-acoustic analysis*, K.U.Leuven, division PMA, PhD thesis 98D12, Leuven, (1998).

[8] E. Trefftz, *Ein gegenstuck zum Ritzschen Verfahren*, in *Proceedings of the 2nd International Congress on Applied Mechanics*, Zürich, Switzerland (1929), pp.131-137.

[9] E. Deckers, N.-E. Hörlin, D. Vandepitte, W. Desmet, *A novel wave based prediction technique for the efficient dynamic modelling of poro-elastic materials*, in *Proceedings of Euronoise, Edinburgh*, Scotland, (2009).

[10] E. Deckers, N.-E. Hörlin, D. Vandepitte, W. Desmet, *A novel wave based method for the efficient 2D dynamic modelling of the poro-elastic Biot equations*, Submitted for publication in Compututational . Methods Appl. Mech. Engrg. (2010).

[11] C. Vanmaele, D. Vandepitte, W. Desmet, *An efficient Wave Based prediction technique for dynamic plate bending problems with corner stress singularities*, Comput. Methods Appl. Mech. Engrg., Vol. 198 (2009), pp. 2227-2245.

[12] C. Vanmaele, K. Vergote, D. Vandepitte, W. Desmet, *An efficient wave based prediction technique for dynamic plate membrane problems*, Submitted for publication in Comput. Methods Appl. Mech. Engrg. (2010).

[13] B. Van Genechten, K. Vergote, D. Vandepitte, W. Desmet, *A multi-level wave based numerical modelling framework for the steady-state dynamic analysis of bounded Helmholtz problems with multiple inclusions*, Comput. Methods Appl. Mech. Engrg., Vol. 199 (2010), pp. 1881-1905.

[14] G.B. Sinclair, *Stress singularities in classical elasticity - I: Removal, interpretation and analysis*, Applied Mechanics Reviews, Vol. 57 (2004), pp. 251-297.

[15] G.B. Sinclair, *Stress singularities in classical elasticity - II: Asymptotic identification*, Applied Mechanics Reviews, Vol. 57 (2004), pp. 385-439.

[16] P. Moon and D.E. Spencer, *Field Theory Handbook Including Coordinate Systems, Differential Equations And Their Solutions*, Springer-Verlag, (1961).

[17] M.D. Greenberg, *Advanced Engineering Mathematics, second edition*, Prentice Hall, New Jersey, (1998).

A Biot theory parameters and nomenclature

	Description	Mathematical formula
b	Viscous drag coefficient	$b = \sigma_{res} h^2 G_J(\omega)$
B^2	Prandtl number	$B^2 = \frac{c_p \mu_f}{k}$
c	Speed of sound	$c = \sqrt{\gamma R^{gas} T}$
c_p	Specific heat	
$e^f(\mathbf{r})$	Volumetric strain in the fluid	$e^f(\mathbf{r}) = \nabla \mathbf{u^f}(\mathbf{r})$
$\mathbf{e^s}(\mathbf{r})$	Solid strain tensor	$\mathbf{e^s}(\mathbf{r}) = \frac{1}{2}(\nabla \mathbf{u}(\mathbf{r}) + (\nabla \mathbf{u}(\mathbf{r}))^T)$
$e^s(\mathbf{r})$	Volumetric strain in the solid	$e^s(\mathbf{r}) = \nabla \mathbf{u^s}(\mathbf{r})$
$e_1^s(\mathbf{r})$	Volumetric strain according to k_{l_1}	
$e_2^s(\mathbf{r})$	Volumetric strain according to k_{l_2}	
E	In-vacuo modulus of elasticity of the bulk solid phase	$E = E_s(1 + j\eta_l)$
G_J	Extra variable to take into account effective density and bulk modulus	$G_J = \sqrt{1 + \frac{4j\alpha_\infty^2 \mu_f \rho_f \omega}{\sigma_{res}^2 h^2 Lambda^2}}$
h	Porosity	
k	conductivity of air	
k_{l_1}	Wave number of 1^{st} compressional wave type	equation (18)
k_{l_2}	Wave number of 2^{nd} compressional wave type	equation (18)
k_t	Wave number of shear wave type	equation (19)
K_a	Adiabatic Bulk modulus of the fluid	$K_a = \gamma R^{gas} T \rho_f$
K_f	Corrected Bulk modulus	$K_f = \frac{K_a}{\beta}$
N	Shear modulus of the frame material	$N = \frac{E}{2(1+\nu)}$
$p(\mathbf{r})$	Average fluid pore pressure	
Q	Compressional coupling factor	$Q = (1-h)K_f$
R	Homogenized bulk modulus of the fluid phase	$R = hK_f$
R^{gas}	Gas constant of air	
T	Temperature	
$\mathbf{u^f}(\mathbf{r})$	Mean macroscopic fluid displacement vector	
$\mathbf{u^s}(\mathbf{r})$	Mean macroscopic solid displacement vector	
α_∞	tortuosity	
β	Correction factor	$\beta = \gamma - \frac{\gamma - 1}{1 + \frac{8\mu_f}{j\Lambda'^2 B^2 \omega \rho_f} \sqrt{1 + j\rho_f \frac{\omega B^2 \Lambda'^2}{16\mu_f}}}$
η_l	Loss factor	
γ	Ratio of specific heats	
λ	Static first Lamé coefficient of the frame material	$\lambda = \frac{E\nu}{(1+\nu)(1-2\nu)}$
Λ	Viscous characteristic length	
Λ'	Thermal characteristic length	
μ_f	Fluid dynamic viscosity	$\mu_f = \rho_f \nu_f$
$\mu_{k_{l_1}}$	scaling constant	$\mu_{k_{l_1}} = \frac{(2N+\lambda+Q^2)k_{l_1}^2 - \omega^2 \rho_{11}^*}{\omega^2 \rho_{12}^* - Q k_{l_1}^2}$
$\mu_{k_{l_2}}$	scaling constant	$\mu_{k_{l_2}} = \frac{(2N+\lambda+Q^2)k_{l_2}^2 - \omega^2 \rho_{11}^*}{\omega^2 \rho_{12}^* - Q k_{l_2}^2}$
μ_{k_t}	scaling constant	$\mu_{k_t} = -\frac{\rho_{12}^*}{\rho_{22}^*}$
ν	Poisson coefficient of the frame material	
ρ_1	Bulk frame mass density	$\rho_1 = (1-h)\rho_s$
ρ_2	Bulk fluid mass density	$\rho_2 = h\rho_s$
ρ_{11}^*	Effective frame mass density with viscous dissipation	$\rho_{11}^* = \rho_1 + \rho_a + \frac{b}{j\omega}$
ρ_{12}^*	Inertial mass coupling factor with viscous dissipation	$\rho_{12}^* = -\rho_a - \frac{b}{j\omega}$
ρ_{22}^*	Effective fluid mass density with viscous dissipation	$\rho_{22}^* = \rho_2 + \rho_a + \frac{b}{j\omega}$
ρ_a	Inertial coupling term	$\rho_a = \rho_f \phi(\alpha_\infty - 1)$
ρ_f	Fluid density	
ρ_s	Mass density of the frame material	
$\sigma^f(\mathbf{r})$	Fluid stress tensor	
$\sigma^s(\mathbf{r})$	Fluid stress tensor	
σ_{res}	Static flow resistivity	
$\Omega^s(\mathbf{r})$	Rotational strain of the solid phase	$\Omega^s(\mathbf{r}) = \nabla \times \mathbf{u^s}(\mathbf{r})$

Table 4: Notations used in the Biot equations